Atomic Layer Deposition of Indium Tin Oxide Thin Films Using Nonhalogenated Precursors

Jeffrey W. Elam,*,† David A. Baker,† Alex B. F. Martinson,†,‡ Michael J. Pellin,† and Joseph T. Hupp‡

Energy Systems Division, Argonne National Laboratory, 9700 South Cass Avenue, Argonne, Illinois 60439, and Department of Chemistry, Northwestern University, 2145 Sheridan Road, Evanston, Illinois 60208

Received: October 4, 2007; In Final Form: November 8, 2007

This article describes a new atomic layer deposition (ALD) method for preparing indium tin oxide (ITO) thin films using nonhalogenated precursors. The indium oxide (In_2O_3) was deposited using alternating exposures to cyclopentadienyl indium (InCp) and ozone, and the tin oxide (SnO_2) used alternating exposures to tetrakis-(dimethylamino) tin (TDMASn) and hydrogen peroxide. By adjusting the relative number of In_2O_3 and SnO_2 ALD cycles, we deposited ITO films with well-controlled SnO_2 content. The ITO films were examined using four-point probe and Hall probe measurements, spectrophotometry, ellipsometry, scanning electron microscopy, atomic force microscopy, X-ray fluorescence, and X-ray diffraction. The lowest resistivity (3×10^{-4} Ωcm) and highest optical transparency (92%) were obtained for films containing 5% SnO_2. The ITO films were slightly thinner and contained more SnO_2 than expected on the basis of rule-of-mixtures predictions. In situ measurements revealed that these discrepancies result from an inhibition of the In_2O_3 growth following the SnO_2 doping layers. This new ALD method is suitable for applying ITO layers on very high aspect ratio nanoporous membranes to be used in photovoltaic or spectroelectrochemical applications.

Introduction

Indium tin oxide (ITO) is a transparent conducting oxide material with a wide range of uses. Thin films of ITO are used in transparent electrodes for flat panel displays, light-emitting diodes, and solar cells. ITO is also used as a heat-reflecting layer to improve the energy efficiency of architectural glass. ITO thin films can be deposited in a variety of ways including sputtering,[1] spray pyrolysis,[2] sol−gel methods,[3] chemical vapor deposition,[4] pulsed laser deposition,[5] and atomic layer deposition (ALD).[6−8] ALD is a thin film growth method utilizing alternating, self-limiting chemical reactions between gaseous precursors and a solid surface to deposit materials in an atomic layer-by-layer fashion.[9] This method can produce films with exquisite control over thickness and composition and allows precise coatings to be applied on all exposed surfaces of nanoporous substrates such as aerogels[10] or mesoporous membranes.[11,12]

ALD ITO films have been prepared previously using $InCl_3$, $SnCl_4$, and either H_2O[7] or H_2O_2[8] as the oxygen source. However, this method suffers from limitations including low growth rates, high deposition temperatures, low volatility of $InCl_3$, and the inconvenience of using halogenated precursors. The chlorinated precursors as well as the HCl byproduct are corrosive and can etch the substrates and damage the deposition equipment. For instance, large exposures to $InCl_3$ can etch the deposited In_2O_3.[6] This behavior is especially problematic when trying to infiltrate porous substrates where large reactant exposures are needed to ensure diffusion throughout the substrate.[12] Finally, halogenated precursors can form agglomerates during large exposures, leading to nonuniform deposits.[13]

We have recently started using ALD techniques to apply metal oxide coatings onto porous supports such as anodic aluminum oxide (AAO) membranes to synthesize dye-sensitized solar cells.[14] As part of this effort, we have developed new methods for depositing ALD In_2O_3 films using alternating exposures to cyclopentadienyl indium (InCp) and ozone[15] and also SnO_2 films using alternating exposures to tetrakis(dimethylamino) tin (TDMASn) and H_2O_2.[16] In this article, we demonstrate how the ALD procedures for In_2O_3 and SnO_2 can be combined to make ITO thin films. We use in situ quartz crystal microbalance (QCM) and quadrupole mass spectrometry (QMS) measurements to investigate the ALD growth mechanism. ITO films are deposited onto Si(100) and glass substrates and examined using variable-angle spectroscopic ellipsometry (VASE), optical transmittance, four-point probe and Hall probe measurements, atomic force microscopy (AFM), scanning electron microscopy (SEM), X-ray fluorescence (XRF), and X-ray diffraction (XRD). Finally, we demonstrate that these methods are capable of conformally coating very high aspect ratio AAO membranes suitable for solar cell electrodes.

Experimental Section

The ALD experiments used a viscous flow reactor[17] constructed from a circular, stainless steel flow tube with an inside diameter of 5 cm to hold the substrates for film growth as well as the QCM. Ultrahigh purity (99.999%) nitrogen carrier gas continuously passed through the flow tube at a mass flow rate of 360 sccm and a pressure of 1 Torr. A constant reactor temperature was maintained by temperature controllers connected to resistive heaters attached to the outside of the reactor. Four separate heating zones were used to establish a uniform temperature profile along the length of the flow tube to minimize artifacts caused by temperature transients during the QCM measurements.[18]

* Corresponding author. E-mail: jelam@anl.gov.
† Argonne National Laboratory.
‡ Northwestern University.

10.1021/jp7097312 CCC: $40.75 © 2008 American Chemical Society
Published on Web 01/23/2008

SnO_2 ALD was performed using alternating exposures to TDMASn (Gelest, >95% purity) and hydrogen peroxide (H_2O_2, Aldrich, 50 wt % in water). In_2O_3 ALD was performed using alternating exposures to InCp (Strem, electronic grade 99.999+% In) and ozone. The ozone was produced using a commercial ozone generator (Ozone Engineering L11) using a feed of ultrahigh purity oxygen at a flow rate of 400 sccm to produce ~10% ozone in oxygen. The TDMASn and InCp were held in separate stainless steel bubblers maintained at 40 °C, and the tubing connecting the bubblers to the ALD reactor was heated to 150 °C to prevent condensation of the precursors on the reactor walls. Ultrahigh purity nitrogen at a mass flow rate of 60 sccm was sent through the bubblers during the reactant exposures and was diverted to bypass the bubblers following the reactant exposures.

The ALD timing sequences can be expressed as $t1-t2-t3-t4$ where $t1$ is the exposure time for the first precursor, $t2$ is the purge time following the first exposure, $t3$ is the exposure time for the second precursor, and $t4$ is the purge time following the exposure to the second precursor with units in seconds. On the basis of our previous studies, the timing sequence used for In_2O_3 ALD was 2−4−2−2, and the timing sequence used for SnO_2 ALD was 1−5−1−5. ITO ALD was accomplished by alternating between the InCp/O_3 cycles for In_2O_3 ALD and the TDMASn/H_2O_2 cycles for SnO_2 ALD. The composition of the films was controlled by adjusting the percentage of SnO_2 cycles that were substituted for In_2O_3 cycles.

To enable in situ measurements during the ITO ALD, a QCM was installed in the ALD reactor in place of the substrates. These studies utilized a Maxtek BSH-150 bakeable sensor, AT-cut quartz sensor crystals with a polished front surface (Colorado Crystal Corporation, part no. CCAT1BK-1007-000), and a Maxtek TM400 film thickness monitor interfaced to a personal computer. The ALD reactor was also equipped with a QMS (Stanford Research Systems RGA300) located downstream of the QCM in a differentially pumped chamber separated from the reactor tube by a 35-μm orifice and evacuated using a 50 L/s turbomolecular pump.

The ALD films were deposited on 2 × 2 cm^2 Si(100) and glass substrates. Before loading, the substrates were cleaned in an ultrasonicator using acetone and then 2-propanol and blown dry using nitrogen. After loading, the substrates were allowed to outgas in the ALD reactor for 10 min at the deposition temperature (typically 275 °C) in 1 Torr of flowing ultrahigh purity nitrogen. Next, the substrates were cleaned in situ using a 60-s exposure to 10% ozone in oxygen at a pressure of 2 Torr and a mass flow rate of 400 sccm.

In our previous study of In_2O_3 ALD, we observed a reactor conditioning effect in which the thicknesses of In_2O_3 films deposited immediately following the growth of a different material, such as Al_2O_3 or SnO_2, were thinner than expected.[15] To compensate for this effect, we always deposited an In_2O_3 buffer layer on the inside of the reactor using ~100 InCp/O_3 cycles following deposition of a different material. After depositing this buffer layer, we proceeded with the ITO deposition experiments.

SEM images were acquired using a Hitachi S4700 with a field emission gun electron beam source. AFM measurements were performed on a Digital Instruments Dimension 3000 with a NanoScope IIIa controller operated in tapping mode. XRD measurements were taken on a Rigaku Miniflex Plus diffractometer. Ellipsometric measurements were performed using a J. A. Woolam Co. M2000V VASE to determine the thickness and refractive index of the ITO films deposited on Si(100) substrates. Optical absorption spectra were acquired from ALD ITO films deposited on glass using the M2000V operated in transmission mode. The resistivities of the ALD ITO films deposited on glass were determined using a four-point probe, and the carrier concentration and mobility were evaluated using a Hall effect measurement system (Ecopia HMS-3000).

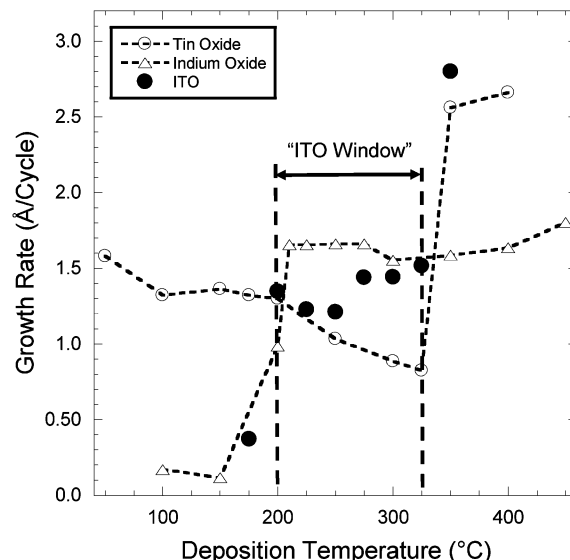

Figure 1. ALD growth rates for In_2O_3 (△), SnO_2 (○), and ITO (●) versus deposition temperature. Potential ALD window for ITO growth is indicated.

XRF measurements were performed using an Oxford Instruments ED2000 to determine the Sn and In contents of the ALD ITO films. To calibrate the XRF signals, a series of pure SnO_2 and In_2O_3 films were prepared on Si(100) substrates and the thicknesses of these films were determined using VASE measurements. Next, the Sn and In signals from these films were measured by XRF. By plotting the XRF signals for Sn and In versus the corresponding SnO_2 and In_2O_3 film thicknesses measured using VASE, we obtained the calibration factors (XRF counts/Å) for Sn and In. These calibration factors were used to extract the effective thicknesses of SnO_2 and In_2O_3 from XRF measurements performed on the ITO films, and the Sn and In contents were calculated using the known atomic densities of these materials.

AAO membranes (Whatman Anodisc 13) were also coated by ITO to evaluate the suitability of the new ALD ITO technique to conformally coat porous materials. The AAO membranes had a thickness of 70 μm and a pore diameter d = 200 nm across most of the membrane thickness which transitioned to a 1−2-μm thick layer with d = 20 nm pores. Cross-sectional SEM analysis was performed on cleaved specimens of the coated AAO membranes.

Results and Discussion

A. Growth of ITO Films. To deposit a mixed-oxide material such as ITO by ALD, it must be possible to deposit the component oxides (In_2O_3 and SnO_2) at a common temperature or range of temperatures. In other words, the ALD temperature "windows" for the component materials must overlap. Figure 1 shows that In_2O_3 can be deposited between 200 and 450 °C.[15] At lower temperatures the O_3 decomposition shuts off, thereby preventing deposition, and at higher temperatures the InCp decomposes. SnO_2 can be deposited between 50 and 325 °C.[16] The lower temperature limit is fixed by the TDMASn vaporization temperature of 40 °C, while at higher temperatures the

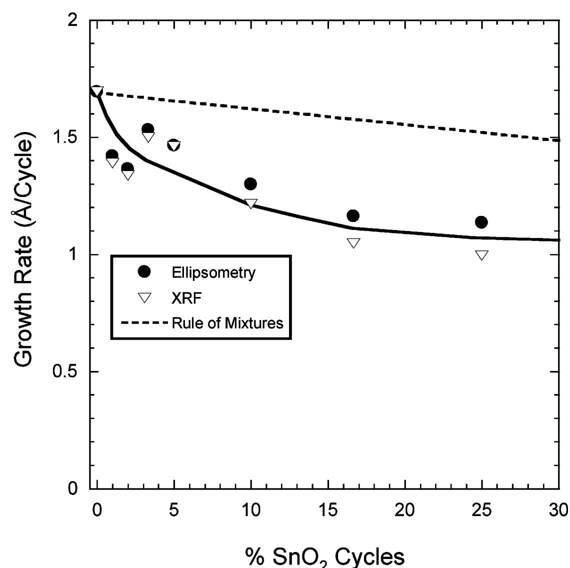

Figure 2. Growth rate for ALD ITO versus percentage of SnO_2 cycles determined using VASE (●) and XRF (▽). Solid line guides the eye, and dashed line shows expected growth rates calculated using a rule-of-mixtures formula.

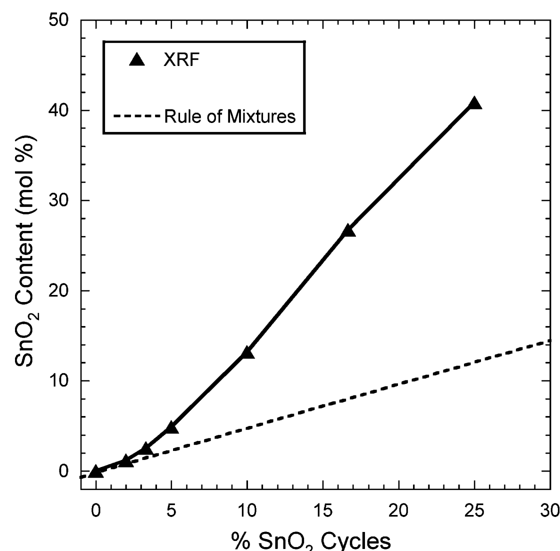

Figure 3. SnO_2 content versus percentage of SnO_2 cycles for ALD ITO films determined by XRF. Dashed line shows expected SnO_2 content as calculated using a rule-of-mixtures formula.

TDMASn begins to decompose. As Figure 1 shows, there should be a temperature window for ITO ALD between 200 and 325 °C. Consequently, a deposition temperature of 275 °C was selected for the initial experiments.

A series of ITO films were prepared on Si(100) using 300 ALD cycles at 275 °C in which the percentage of SnO_2 cycles was varied between 0 and 25%. The total thicknesses of these films were determined using VASE measurements, and the effective thicknesses of SnO_2 and In_2O_3 for the films were calculated from XRF measurements using the calibration procedure described in the Experimental Section. The ITO growth rates determined from the VASE and XRF results are given by the circles and triangles, respectively, in Figure 2, and the solid line guides the eye. The ITO growth rate decreases steadily from 1.69 Å/cycle for 0% SnO_2 to 1.07 Å/cycle for 25% SnO_2. There is fairly good agreement between the VASE and XRF growth rate measurements for these ITO films. The dashed line in Figure 2 shows the anticipated ITO growth rates based on a rule-of-mixtures formula and reveals that the measured growth rates are below the rule-of-mixture estimates for all of the ITO films.

Figure 3 presents the SnO_2 mol % for the ITO films versus the percentage of SnO_2 cycles as determined by XRF. The SnO_2 content increases steadily from 1.2 mol % SnO_2 at 2% SnO_2 cycles to 41 mol % SnO_2 at 25% SnO_2 cycles. The dashed line in Figure 3 shows the expected SnO_2 content based on a rule-of-mixtures formula. Over the entire range of SnO_2 cycles, the SnO_2 content is higher than the predicted values.

In situ QCM and QMS measurements were performed to investigate the discrepancies in thickness and composition. Figure 4 shows the QCM signals recorded during the ALD of ITO using 10% SnO_2 cycles at 275 °C. This figure plots the growth rate measured during each ALD cycle assuming densities of 7.19 and 6.95 g/cm^3 for the In_2O_3 and SnO_2, respectively. Although the steady-state growth rate measured for In_2O_3 using the QCM is ~1.4 Å/cycle, the In_2O_3 growth rate drops to ~1 Å/cycle after each SnO_2 cycle. Following the SnO_2 cycles, the In_2O_3 growth rate increases toward the steady-state value over the following 5−7 cycles. Apparently, the SnO_2 temporarily inhibits the In_2O_3 growth.

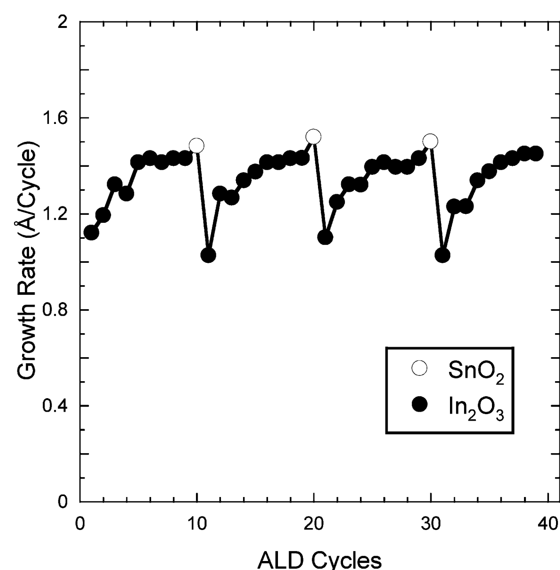

Figure 4. Growth rate versus ALD cycles measured using in situ QCM during ITO growth using 10% SnO_2 cycles.

Next, QMS experiments were performed to explore the origin for the inhibited In_2O_3 growth following the SnO_2 cycles. Figure 5a shows the $m = 66$ signal from cyclopentadiene versus time measured during the ALD of ITO using 5% SnO_2 cycles at 275 °C. The TDMASn exposures for each SnO_2 cycle are indicated in the figure. Cyclopentadiene is released exclusively during the InCp exposures, and the magnitude of the $m = 66$ signal is proportional to the amount of In_2O_3 deposited during each ALD cycle.[15] In agreement with the QCM measurements, Figure 5a shows that the In_2O_3 growth rate decreases substantially following each SnO_2 cycle, and 8−12 In_2O_3 cycles are required for the In_2O_3 growth rate to recover to the steady-state value.

Figure 5b presents the $m = 48$ signal for O_3 that was recorded simultaneously with the $m = 66$ data in Figure 5a. No O_3 is observed during the In_2O_3 ALD when the In_2O_3 growth rate has reached the steady-state value. This observation is consistent with our previous finding that O_3 decomposes on the In_2O_3 very efficiently, and this decomposition is necessary for the In_2O_3 growth.[15] Curiously, the $m = 48$ signal returns during the O_3

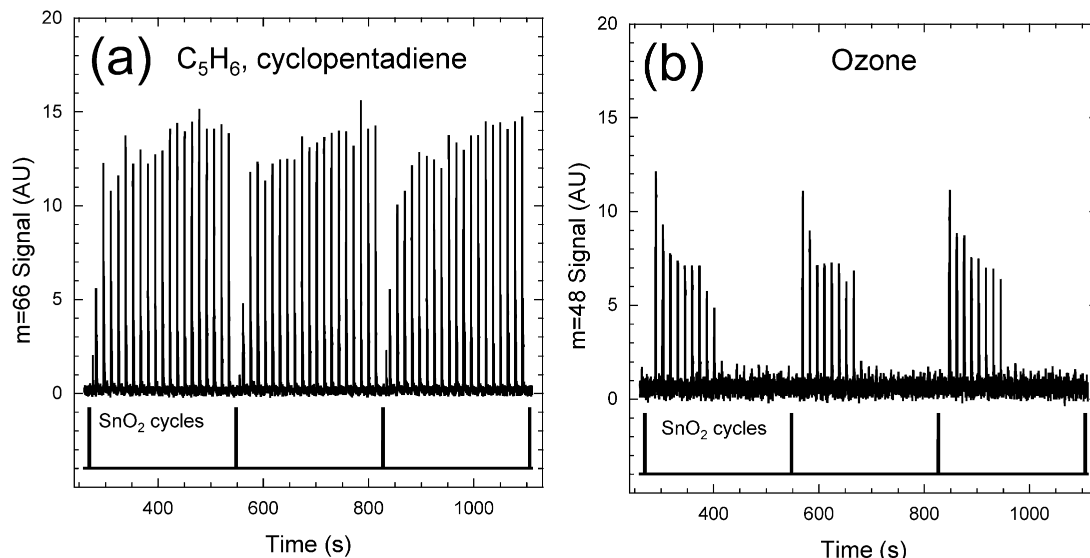

Figure 5. In situ QMS measurements for (a) $m = 66$ from cyclopentadiene and (b) $m = 48$ from ozone, measured during ITO ALD using 5% SnO_2 cycles. The application of the SnO_2 ALD cycles is indicated.

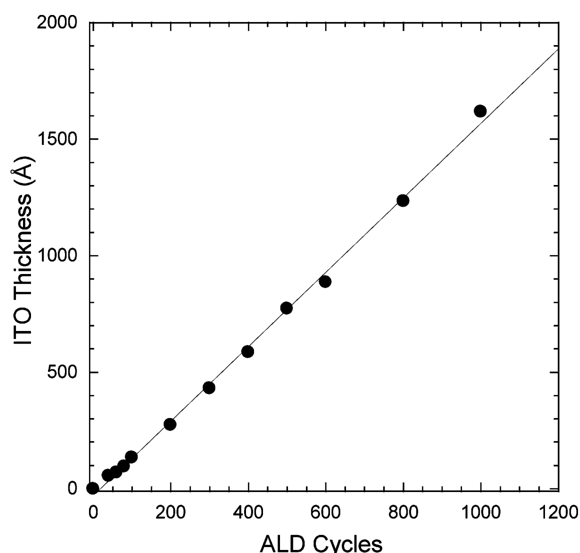

Figure 6. Thickness of ALD ITO films versus number of cycles determined using VASE for films deposited on Si(100) at 275 °C using 5% SnO_2 cycles.

exposures that immediately follow the SnO_2 ALD cycles, and this O_3 signal persists for approximately 8−10 cycles.

Figures 4 and 5 demonstrate that the SnO_2 cycles inhibit the subsequent In_2O_3 ALD, and this may result from the suppression of O_3 decomposition by the SnO_2. In our previous In_2O_3 ALD study, we observed a reactor conditioning effect in which the thicknesses of In_2O_3 films deposited immediately following Al_2O_3 growth were thinner than expected. To compensate for this effect, we always deposited an In_2O_3 buffer layer on the inside of the reactor following deposition of a different material. Evidently, the SnO_2 deposited during a single SnO_2 cycle is sufficient to suppress the O_3 decomposition necessary to sustain the In_2O_3 growth. The reduced In_2O_3 growth observed using QCM and QMS explains why the ITO films are thinner than expected (Figure 2), and also why the ITO films contain more SnO_2 than expected (Figure 3).

Despite the peculiar effect of the SnO_2 on the In_2O_3 ALD, it is still possible to deposit ITO films with excellent control over film thickness and SnO_2 content. Figure 6 shows the ITO thickness versus the number of ALD cycles measured using VASE for films prepared with 5% SnO_2 cycles at 275 °C. This plot yields a growth rate for ITO of 1.60 Å/cycle. This value is substantially larger than the growth rates of 0.20−0.32 Å/cycle measured previously for the ALD of ITO using halogenated precursors.[8] A more detailed examination of the thickness data in Figure 6 reveals that the ITO growth rate increases slightly with the number of ALD cycles from 1.35 Å/cycle at 50 cycles to 1.65 Å/cycle at 1000 cycles. Gradual changes in ALD growth rates have been observed previously for nanocrystalline materials in which the morphology or crystal size evolves with film thickness.[15,19,20]

The filled circles in Figure 1 show the ITO growth rate versus the deposition temperature measured by VASE for films prepared using 300 cycles with 5% SnO_2 cycles. Figure 1 demonstrates that the experimentally determined temperature window for ITO ALD matches very closely with the temperature range predicted from the component oxides. In particular, the ITO growth rate remains nearly constant at 1.35−1.51 Å/cycle in the temperature range 200−325 °C. The ITO growth rate falls off below 200 °C, and this probably results from the abrupt onset of O_3 decomposition at 200 °C.[15] The ITO growth rate increases substantially above 325 °C, and this undoubtedly signals the TDMASn thermal decomposition.[16]

B. Properties of ITO Films. Once the growth behavior of the ALD ITO films was understood, we proceeded to measure the properties of the films to determine the effect of the deposition conditions on the resistivity, transparency, and morphology of the ITO. Figure 7a shows the ITO resistivity versus percent SnO_2 cycles determined using four-point probe measurements of films prepared on glass at 275 °C using 300 ALD cycles. Initially, the ITO resistivity decreases dramatically from 1.4×10^{-2} Ωcm at 0% SnO_2 cycles to 3.9×10^{-4} Ωcm at 5% SnO_2 cycles, and then increases slightly to 1.1×10^{-3} Ωcm at 25% SnO_2 cycles.

Hall probe measurements performed on the samples prepared on glass confirmed that the ITO films are n-doped, and the Hall probe resistivity values were nearly identical to those obtained using the four-point probe. The carrier concentration and mobility values obtained using the Hall probe (Figure 7b) reveal that the decrease in resistivity with SnO_2 doping can be mostly attributed to an increase in carrier concentration. The carrier concentration increases from 1.3×10^{19} cm^{-3} at 0% SnO_2 cycles to 4.0×10^{20} cm^{-3} at 5% SnO_2 cycles. In contrast, the mobility

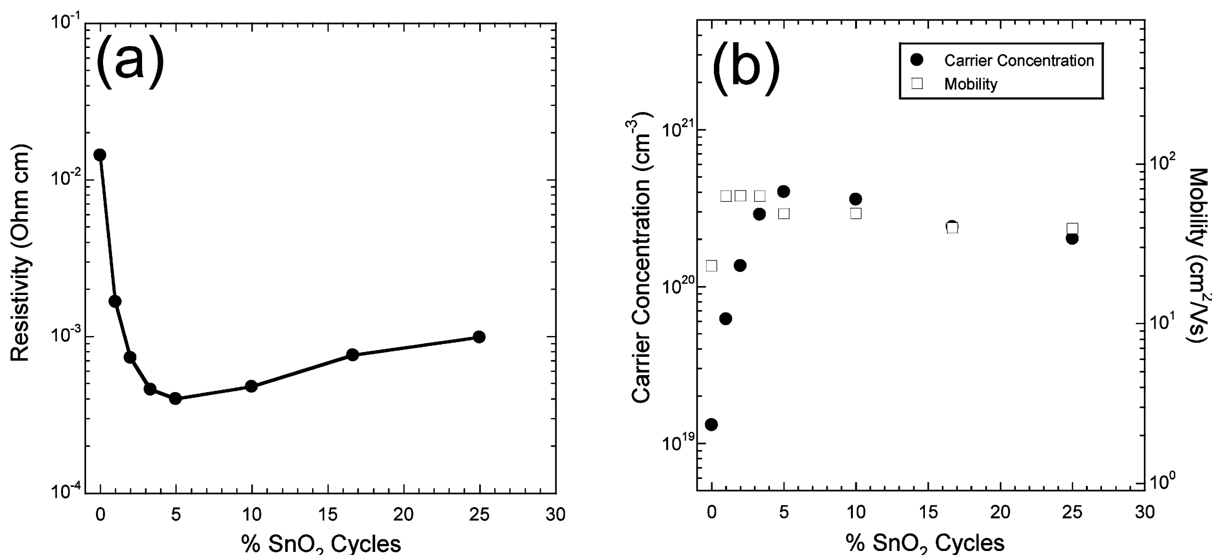

Figure 7. (a) Resistivity versus percentage of SnO_2 cycles measured using four-point probe for ALD ITO films prepared on glass at 275 °C using 300 cycles. (b) Hall probe measurements of the same ITO films showing carrier concentration and mobility.

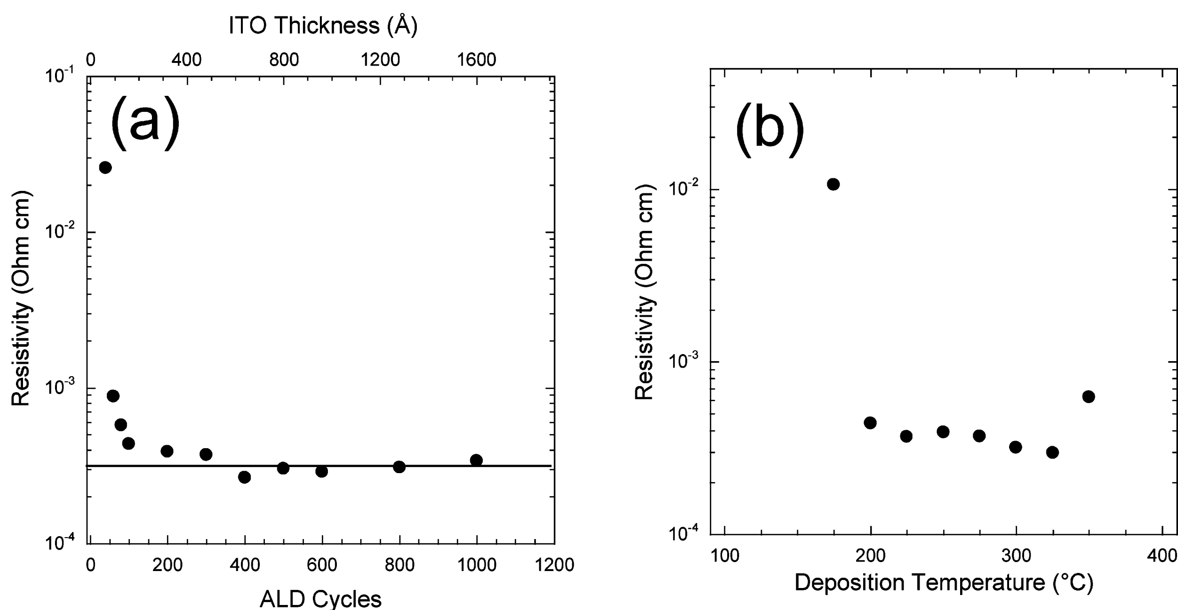

Figure 8. Resistivity of ALD ITO films prepared on glass using 5% SnO_2 cycles measured by four-point probe versus (a) number of cycles at 275 °C and (b) deposition temperature using 300 cycles.

only increases from 23 to 49 cm^2/Vs over this range. The mobility of the undoped In_2O_3 is unusually low; however, this film is only 51-nm thick and In_2O_3 mobilities are thickness-dependent.[21] We measure a more typical mobility of 72 cm^2/Vs for an In_2O_3 with a thicknkess of 200 nm. The electrical characteristics of the ITO films prepared using 5% SnO_2 cycles in this study are comparable to values obtained for ALD ITO films deposited previously using metal chloride precursors.[7] In addition, these electrical transport values are very similar to the values measured for commercially available ITO films prepared using sputtering.

It is interesting to compare the carrier concentration determined by the Hall probe measurements with the actual concentration of Sn atoms in the ITO films measured by XRF. The ratio of these values is known as the doping efficiency, where a value of 100% implies that every Sn atom contributes one free electron. For the ITO film prepared using 5% SnO_2 cycles, the Hall probe measured a carrier concentration $n = 4.0 \times 10^{20}$ cm^{-3}, while XRF yielded 4.9% SnO_2 for this film. Using the atomic density of bulk In_2O_3, this composition corresponds to a Sn atom density of 7.6×10^{20} cm^{-3} so that the doping efficiency is 53%. This number compares favorably with ITO films of similar Sn content prepared by sol−gel techniques.[3] It is thought that the remaining 47% of the Sn atoms forms neutral clusters such as Sn_2O_4 that do not contribute to the ITO conductivity.[22] Perhaps by doping the In_2O_3 using a different SnO_2 precursor with a lower growth rate than TDMASn, the Sn atoms could be spaced farther apart to avoid forming neutral clusters, thereby increasing the doping efficiency.

Next, the ITO resistivity was evaluated versus the film thickness and deposition temperature. The resistivity of the ITO films prepared on glass at 275 °C using 5% SnO_2 cycles was measured by four-point probe versus the number of ITO cycles as shown in Figure 8a. The ITO resistivity remains relatively constant at 2.7×10^{-4} to 4.4×10^{-4} Ωcm over the range 100−1000 ALD cycles. This range corresponds to ITO thicknesses of 13−162 nm. Only at very small numbers of ALD cycles does the resistivity of the ITO increase, and for 40 cycles (5.6 nm) the resistivity reaches 2.6×10^{-2} Ωcm. The ITO resistivity

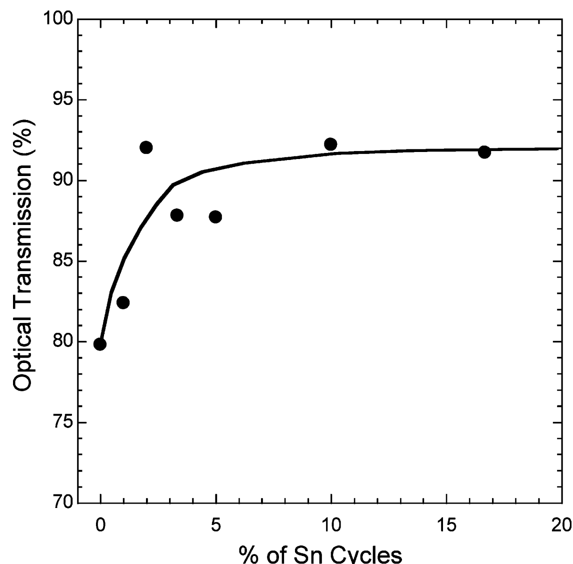

Figure 9. Optical transmittance for ALD ITO films prepared on glass using 300 ALD cycles with 5% SnO_2 cycles versus deposition temperature. Optical transmittance is given as the average transmission over the wavelength range 370−1000 nm.

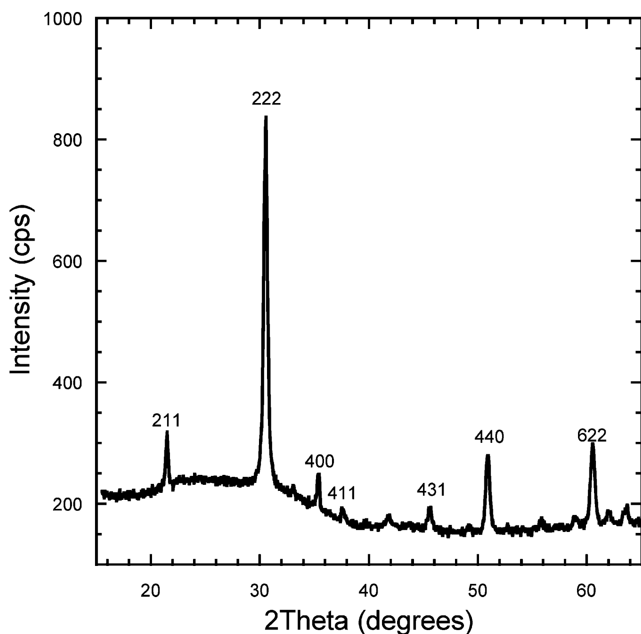

Figure 10. X-ray diffraction profile measured for ALD ITO film deposited on glass using 1000 cycles with 5% SnO_2 cycles at 275 °C. The indices and peak positions are taken from PDF No. 00-006-0416 for cubic In_2O_3.

was also measured by four-point probe as a function of the deposition temperature for films deposited on glass using 300 ALD cycles with 5% SnO_2 cycles. Figure 8b demonstrates that the ITO resistivity decreases slightly with increasing deposition temperature from 4.4×10^{-4} to 3.0×10^{-4} Ωcm between 225 and 350 °C. The increase in resistivity observed at higher temperatures probably results from impurities caused by the TDMASn decomposition. At temperatures below 225 °C, the films are much thinner and probably contain little indium, and thus the resistivity is closer to that of SnO_2.[16]

Figure 9 shows optical transmission measurements for the ITO films prepared on glass as a function of the percentage of SnO_2 cycles obtained by integrating the transmission spectra over the wavelength range 370−1000 nm. The transmission spectra were referenced to an uncoated glass substrate. These films were deposited at 275 °C using 300 ALD cycles. Although the data are somewhat scattered, the overall trend is an increase in transmittance from ~80% at 0% SnO_2 cycles to an average value of ~90% at 16% SnO_2 cycles. The increased transmittance is due in part to a blue shift in the absorption edge of the transmission curves with increasing SnO_2 content known as the Burstein−Moss effect. As the conduction band fills, the Fermi level exceeds the conduction band minimum and a larger photon energy is required for absorption.[23] Alternatively, a decrease in surface roughness with increasing Sn content might reduce optical scattering and produce the effect shown in Figure 9. VASE measurements for the 5% ITO films deposited on Si(100) yielded a refractive index at 633 nm of $n = 1.89$.

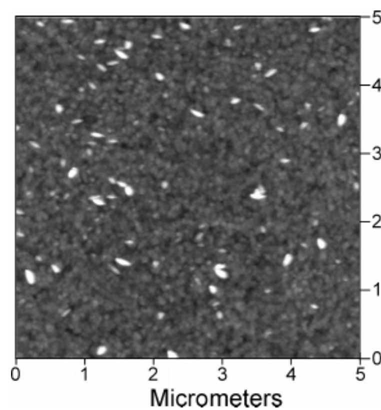

Figure 11. AFM image for 89-nm ALD ITO film deposited on Si(100) at 275 °C using 600 cycles with 5% SnO_2 cycles.

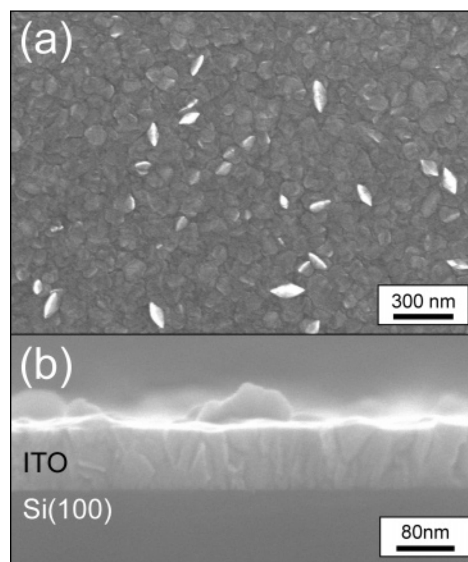

Figure 12. SEM plan-view (a) and cross-sectional (b) images of ALD ITO film deposited on Si(100) using 600 cycles with 5% SnO_2 cycles at 275 °C.

Figure 10 shows the X-ray diffraction profile measured for an ITO film deposited on glass using 1000 ALD cycles with 5% SnO_2 cycles at 275 °C. The indices and peak positions in Figure 10 are taken from PDF No. 00-006-0416 for cubic In_2O_3. The ITO deposits in a polycrystalline form with a cubic In_2O_3 structure, and the most prominent orientation is the [111] direction. Figure 11 shows an AFM image of an ITO film with a thickness of 89 nm deposited at 275 °C using 600 cycles with 5% SnO_2 and yields an rms roughness of 8.9 nm. As expected from the XRD measurements, Figure 11 shows a polycrystalline morphology. In addition, a small number of unusually tall features (10−40 nm) are seen on the surface. These large

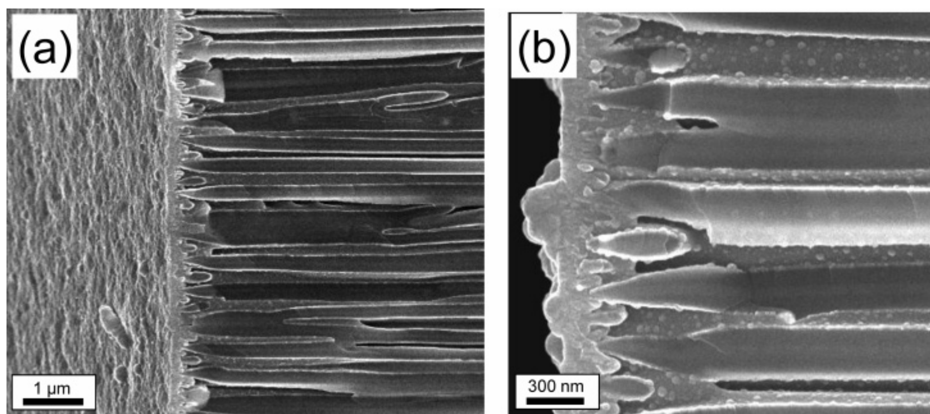

Figure 13. (a) Cross-sectional SEM image of AAO membrane coated conformally with 9.7-nm ALD ITO film, and also with 161-nm ALD ITO film deposited selectively on the AAO front surface visible on the left side of the image. (b) Higher-resolution SEM image of AAO membrane showing that the 20-nm pores are sealed, and ITO nanocrystals decorate the inner walls of the 200-nm pores.

crystals might explain the dominant (222) peak seen in XRD. Previous ALD studies of ITO observed neither the large crystals nor the dominant (222) peak.[7]

Figure 12 shows SEM images of an ALD ITO film prepared on Si(100) using 600 cycles with 5% SnO_2 cycles at 275 °C. The plan-view image (Figure 12a) shows a surface that is uniformly decorated with platelike crystals in addition to taller, diamond-shaped crystals that correspond to the tall features in the AFM image. Additional SEM and AFM measurements showed that the height and number of these tall, diamond-shaped crystals increased with increasing ITO film thickness. The cross-sectional SEM image (Figure 12b) yields an ITO film thickness of 82 ± 8 nm, in good agreement with the thickness of 88.7 nm obtained using VASE.

C. Fabrication of High Surface Area ITO. We used the ALD methods described in the preceding sections to synthesize high surface area transparent, conducting electrodes that could be used in nanostructured photovoltaic[14] or spectrophotochemical[24] applications. First, a thin ITO coating was deposited on a commercial AAO membrane that completely infiltrated the AAO pores to create a conformal, uniform coating with a thickness of 9.7 nm. This process used 58 ALD cycles with 10% SnO_2 cycles at a temperature of 275 °C with the timing sequence 12−10−60−5 for In_2O_3 and 10−10−10−10 for SnO_2. Next, the AAO was mounted in a fixture that limited deposition to the front, 20-nm pore side of the membrane, and an ITO film with a thickness of 161 nm was deposited. The function of this thick layer was to seal off the small pores and also to provide a low resistance contact to the electrode. The thick layer used 1000 cycles with 5% SnO_2 cycles at a temperature of 275 °C with the timing sequence 2−4−2−2 for In_2O_3 and 1−5−1−5 for SnO_2.

Cross-sectional SEM images of the resulting electrode are shown in Figure 13. Figure 13a demonstrates that the 20-nm pores of the membrane are completely sealed, while the underlying 200-nm pores are still open beneath the thick coating. Figure 13b is a higher resolution image showing that the inside surfaces of the pores are decorated with ITO nanocrystals. The coated membrane had a 5 Ω resistance through the membrane, a 15 Ω/□ sheet resistance on the thickly coated side, and an optical transparency of ∼70%.

Conclusions

We have demonstrated a new method for depositing ITO thin films by ALD using alternating $InCp/O_3$ exposures for In_2O_3 and $TDMASn/H_2O_2$ exposures for SnO_2. By adjusting the relative number of In_2O_3 and SnO_2 ALD cycles, we deposited ITO films with precise control over the thickness and SnO_2 content. ITO films with a thickness of 42 nm deposited on glass using 5% SnO_2 cycles exhibited a resistivity of 3×10^{-4} Ωcm and an optical transparency of 92%. The ITO films were slightly thinner and contained more SnO_2 than predicted, and in situ measurements revealed that these discrepancies result from an inhibition of the In_2O_3 growth following the SnO_2 cycles. We have used this new ALD method to apply conformal ITO layers on very high aspect ratio nanoporous membranes.

Acknowledgment. The work at Argonne is supported by the U.S. Department of Energy, BES-Materials Sciences under Contract W-31-109-ENG-38. The work at Northwestern University is supported by the U.S. Department of Energy, Basic Energy Sciences Program under Grant No. DE-FG02-87ER13808. Electron microscopy was performed at the Electron Microscopy Center for Materials Research at Argonne National Laboratory, a U.S. Department of Energy Office of Science Laboratory operated under Contract No. DE-AC02-06CH11357 by UChicago Argonne, LLC.

References and Notes

(1) Calnan, S.; Upadhyaya, H. M.; Thwaites, M. J.; Tiwari, A. N. *Thin Solid Films* **2007**, *515*, 6045.
(2) Rozati, S. M.; Ganj, T. *Renewable Energy* **2004**, *29*, 1671.
(3) Tahar, R. B. H.; Ban, T.; Ohya, Y.; Takahashi, Y. *J. Appl. Phys.* **1998**, *83*, 2139.
(4) Suzuki, A.; Maki, K. *Chem. Vap. Deposition* **2006**, *12*, 608.
(5) Gupta, R. K.; Mamidi, N.; Ghosh, K.; Mishra, S. R.; Kahol, P. K. *J. Optoelectron. Adv. Mater.* **2007**, *9*, 2211.
(6) Asikainen, T.; Ritala, M.; Leskela, M. *J. Electrochem. Soc.* **1994**, *141*, 3210.
(7) Asikainen, T.; Ritala, M.; Leskela, M. *J. Electrochem. Soc.* **1995**, *142*, 3538.
(8) Ritala, M.; Asikainen, T.; Leskela, H. *Electrochem. Solid State Lett.* **1998**, *1*, 156.
(9) Ritala, M.; Leskela, M. Atomic Layer Deposition. In *Handbook of Thin Film Materials;* Nalwa, H. S., Ed.; Academic Press: San Diego, CA, 2001; Vol. 1, p 103.
(10) Kucheyev, S. O.; Biener, J.; Wang, Y. M.; Baumann, T. F.; Wu, K. J.; van Buuren, T.; Hamza, A. V.; Satcher, J. H., Jr.; Elam, J. W.; Pellin, M. J. *Appl. Phys. Lett.* **2005**, *86*, 083108.
(11) Pellin, M. J.; Stair, P. C.; Xiong, G.; Elam, J. W.; Birrell, J.; Curtiss, L.; George, S. M.; Han, C. Y.; Iton, L.; Kung, H.; Kung, M.; Wang, H. H. *Catal. Lett.* **2005**, *102*, 127.
(12) Elam, J. W.; Routkevitch, D.; Mardilovich, P. P.; George, S. M. *Chem. Mater.* **2003**, *15*, 3507.
(13) Puurunen, R. L. *Chem. Vap. Deposition* **2005**, *11*, 79.
(14) Martinson, A. B. F.; Elam, J. W.; Hupp, J. T.; Pellin, M. J. *Nano Lett.* **2007**, 2183.
(15) Elam, J. W.; Martinson, A. B. F.; Pellin, M. J.; Hupp, J. T. *Chem. Mater.* **2006**, *18*, 3571.

(16) Elam, J. W.; Baker, D. A.; Hryn, A. J.; Martinson, A. B. F.; Pellin, M. J.; Hupp, J. T. *J. Vac. Sci. Technol., A*, Accepted, 2007.
(17) Elam, J. W.; Groner, M. D.; George, S. M. *Rev. Sci. Instrum.* **2002**, *73*, 2981.
(18) Rocklein, M. N.; George, S. M. *Anal. Chem.* **2003**, *75*, 4975.
(19) Ritala, M.; Leskela, M.; Nykanen, E.; Soininen, P.; Niinisto, L. *Thin Solid Films* **1993**, *225*, 288.
(20) Elam, J. W.; George, S. M. *Chem. Mater.* **2003**, *15*, 1020.
(21) Suzuki, T.; Yamazaki, T.; Takizawa, M.; Kawasaki, O. *J. Mater. Sci.* **1989**, *24*, 187.
(22) Frank, G.; Kostlin, H. *Appl. Phys. A* **1982**, *27*, 197.
(23) Gupta, L.; Mansingh, A.; Srivastava, P. K. *Thin Solid Films* **1989**, *176*, 33.
(24) Doherty, W. J.; Wysocki, R. J.; Armstrong, N. R.; Saavedra, S. S. *J. Phys. Chem. B* **2006**, *110*, 4900.